GEANT Simulations of DRAGON and the $^{12}C(^{12}C,\gamma)^{24}Mg$ Reaction

Joshua Slater
University of Waterloo
ID 20070583
2B Honours Physics

DRAGON Research Group, TRIUMF
Vancouver, British Columbia

Supervisors: Dave Hutcheon, Michael Trinczek and John D'Auria

May 3^{rd}, 2004

Abstract

GEANT simulations of DRAGON and the radiative capture $^{12}C(^{12}C,\gamma)$ reaction were performed to understand the acceptance efficiencies and BGO response. Significant changes to both the real DRAGON and the simulated DRAGON had to be made: target cell changes for the solid target experiments, and collimator and pumping tube changes for better recoil detection. A new HBOOK ntuple, GAMMAHIT, was added to existing DRAGON simulations for more detailed analysis. Recoil acceptance was calculated to be 42.8% and 8.6% for cascade decays of two 10 MeV gammas and single decays of one 20 MeV gamma, respectively. Differentiating between the two decay paths will be possible with the BGO detector array.

Contents

List of Figures

1 Introduction

1.1 DRAGON

The Detector Of Recoils And Gamma-rays Of Nuclear reactions (DRAGON) is one of the TRI-University Meson Facility's (TRIUMF) facilities for studying nuclear reactions of astrophysical importance. DRAGON is situated on the high energy beam line in the Isotope Separator and ACelerator (ISAC) facility at TRIUMF, which provides high energy beams (0.15 to 1.5 $\frac{MeV}{u}$) of heavy ions to DRAGON, as well as to other experiments. DRAGON uses these heavy ion beams and a gaseous target to study radiative capture reactions, the fusion of beam and target nuclei which cools by gamma emission. These capture reactions, which involve a nucleus capturing hydrogen or helium, are very important astrophysically as they provide important steps in the nucleosynthesis of light elements to heavier elements. DRAGON is composed of two main sections, a target cell surrounded by a gamma detector array and an ElectroMagnetic Separator (EMS) with a heavy ion detector, both of which are described below. A complete layout of DRAGON is displayed in figure 1.

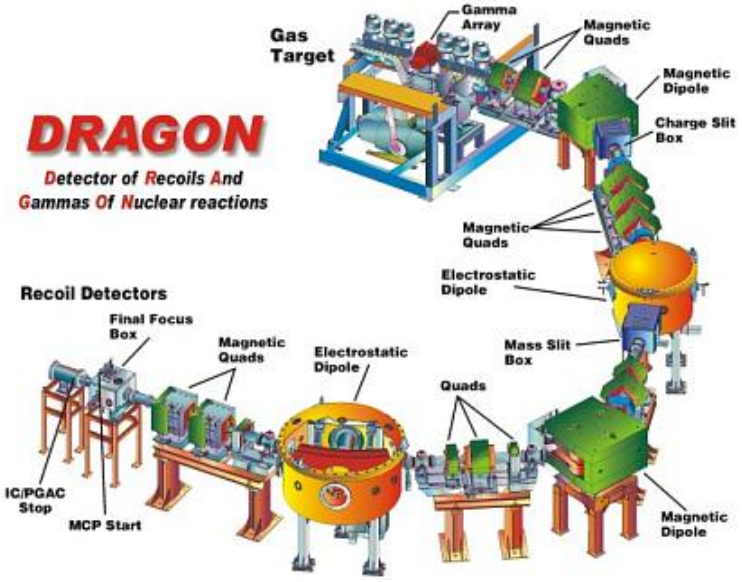

Figure 1: 3D Schematic of DRAGON.

The target area of DRAGON typically has a windowless gas cell filled with either hydrogen or helium gas. A windowless gas cell, as opposed to a thin windowed cell, has the advantage that this eliminates windows that could effect the direction or charge of the incoming beam, making it easier for DRAGON to maximize beam transmission through the target. However, leaky gas escapes from the cell up and down stream of the target area. This is resolved by using a series of tubes and differential pumping. Typical gas pressures fall within the target range from 0.2 Torr to 4 Torr and the pumping tubes reduce the gas pressure to about 10^{-6} Torr at the entrance of the separator. Gas pressures within the 11 cm cell are nearly uniform. The gas cell also contains two solid-state detectors that measure the rate of elastic scattering within the target. They are positioned to detect scattering at a central portion of the target gas. As elastic scattering rates are proportional to the product of gas pressure and beam current, and the gas pressure can be measured independently, the elastic monitors can be used to calculate beam current during a run. The collimators and pumping tubes downstream of the target were originally designed to allow any reaction products or recoils within 20 mrad into the separator but recently built larger tubes have increased this acceptance to 25 mrad.

The target cell is surrounded by a gamma detector array composed of 30 crystal scintillators made of bismuth germanate (BGOs) of hexagonal cross section. The BGOs are stacked around the target and cover the majority of the 4π solid angle, as seen in figure 2. Simulations predict a detection efficiency of 45% to 60% for 1 to 10 MeV gamma rays emitted from within the target. The array was constructed out of BGO because the material follows a simple exponential as it scintillates and does not have any afterglow. It also has one of the highest densities of scintillator material and hence has a very good stopping power, which is important for studying decays that emit high energy gammas. The worst attenuation for BGO is 5 cm for 5 MeV gammas. This was an important factor in the dimensions of the scintillators, which were designed to be 7.6 cm long and 5.6 cm hexagonal shaped cross-section. Each BGO is coupled to a cylindrical photomultiplier tube (PMT).

The EMS section of DRAGON is 21 m long and employs both magnetic and electrostatic components. The first dipole is magnetic and is used to select recoils of a specific charge. The dipole bends charged particles towards a pair of slits, which are positioned to stop unreacted beam particles and recoils of unwanted charge states. The second dipole is an electrostatic dipole

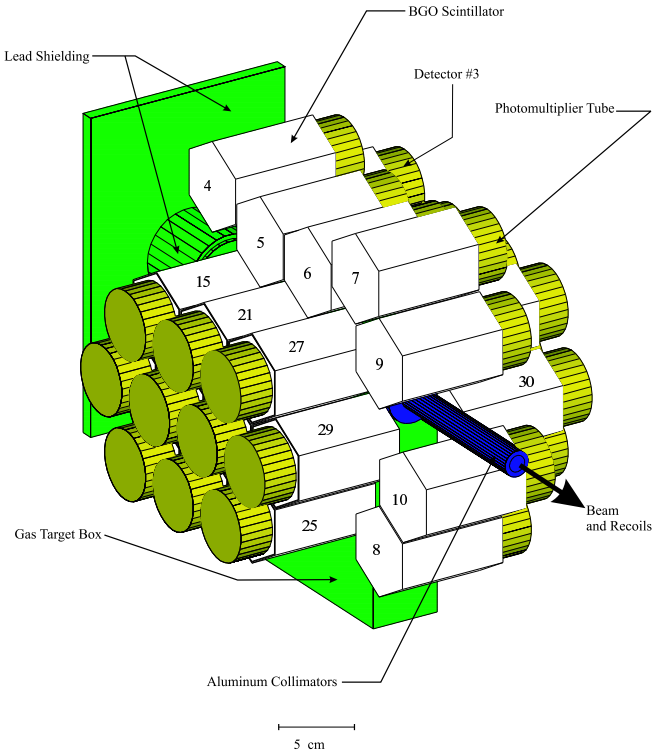

Figure 2: 3D Schematic of BGO Detector Array.

used to select particles by mass. Again, the dipole bends particles towards a pair of slits to separate unwanted particles. A second magnetic dipole and a second electrostatic dipole that bend particles at larger angles follow to form a second phase of separation. A third and final pair of slits is positioned after the second phase of separation. Throughout the separator are magnetic quadrupoles, which focus beam or recoils, and magnetic sextuples, which correct for aberrations. These are used to narrow the beam or recoils as much as possible to achieve a focus at each pair of slits. This enhances transmission of recoils and blocking of beam particles. For each reaction the electromagnetic elements of DRAGON are set with fields, or tuned, which steer the desired recoils through the separator and into the final detectors. There are also four steering magnets in DRAGON that can deflect particles

20 mrad and can be used to straighten crooked beams.

For accurate field measurements both magnetic dipoles contain Nuclear Magnetic Resonance (NMR) probes and all quadrupoles contain Hall probes. The NMR probe in the first magnetic dipole can be used to accurately measure and confirm beam energies, according to the relation

$$E = k(\frac{qB}{A})^2 \quad (1)$$

where E is the energy of the beam in MeV per nucleon, $k = 482.3\frac{MeVu}{kG^2}$, q is the charge of the beam, A is the atomic mass of the beam and B is the field in the first magnetic dipole as measured by the NMR probe.

The EMS contains a vacuum system that pumps out the electrostatic dipoles and three diagnostic boxes. The diagnostic boxes are located before, between and after the two dipoles. Pressure in the dipoles is as low as 10^{-8} Torr when closed off from the rest of the system and 10^{-7} Torr when opened. Each dipole is equipped with three pumps: a turbomolecular pump to pump down from high pressures, a cryopump to pump while the dipoles are running, and an ion pump for when the dipoles are not running to keep them clean.

DRAGON is also equipped with several heavy ion detectors at the end of the separator. The detector used in the experiments discussed herein was a Double-Sided Silicon-Strip Detector (DSSSD), which is a solid state device. The DSSSD has 16 horizontal silicon strips on the front and 16 vertical strips on the back, all with 3 mm pitch, that cover a square 25 cm^2 area. A detected particle creates a pulse in a front and a back strip, from which position and energy can be deduced. There are other available detectors at DRAGON as well. A thin-window ion chamber can be used to measure $\frac{dE}{dx}$ and to calculate particle mass. A fast-timing Micro-Channel Plate (MCP) can be used with another fast-timing detector to make time of flight measurements and also calculate particle mass. When one of these detectors is triggered shortly after the BGO array it is recorded as a coincident event. This is an excellent method to distinguish between recoil particles and non-separated beam particles. More detailed information about DRAGON can be found in the literature [1].

1.2 The $^{12}C(^{12}C,\gamma)^{24}Mg$ Reaction

While DRAGON was designed as a powerful tool for nuclear astrophysics it can also be used in other nuclear physics experiments. The radiative capture experiments typically performed on DRAGON involve light nuclei and are a well-understood process. Radiative capture involving heavy ions (HIRC) is a far less understood process and has mostly been explored with the ^{12}C + ^{12}C $\rightarrow$ ^{24}Mg + γ reaction, abbreviated $^{12}C(^{12}C,\gamma)$ and the $^{12}C(^{16}O,\gamma)$ reaction. Very little work has been done on HIRC since the early 1980s.

The $^{12}C(^{12}C,\gamma)$ reaction is of particular interest because the excited ^{24}Mg nucleus has been explained in terms of nuclear molecules [2]. These theories involve the nucleus behaving as a series of smaller nuclei such as two ^{12}C nuclei, or one ^{12}C and three ^{4}He nuclei, or some other combination, before decaying to the normal compound nucleus. During this decay ^{24}Mg may exist in an intermediate 'doorway' state, which could have the properties of both the nuclear molecule and the compound nucleus. The existence of these 'doorway' states has yet to be confirmed.

Studies have been done on the $^{12}C(^{12}C,\gamma)$ reaction in the past. In particular, Sandorfi and Nathan measured decays of a single high energy gamma to low energy states of ^{24}Mg [3]. They were not able to study cascade decays with multiple low energy gammas that would have passed through the 'doorway' states because these studies employed a single sodium iodide scintillator. The cross section associated with particle decays was around 500 mb whereas radiative capture cross sections were 1 b. This is typically the case for HIRC as there exists a high Coulomb barrier and a positive Q-value, meaning product nuclei are highly excited, typically more than 10 MeV above particle separation energies. In the Sandorfi and Nathan studies, low energy gammas from the highly favoured particle decays of ^{24}Mg flooded their sole detector and prevented the study of radiative cascade decays with multiple low energy gammas. Any study of HIRC is therefore an experimental challenge.

More recent work on the $^{12}C(^{12}C,\gamma)$ reaction by Jenkins used the Gammasphere at Lawrence Berkeley National Laboratory, which contains high-resolution germanium scintillators surrounded by high-efficiency BGO scintillators [4]. These detectors cover the entire 4π solid angle. An accelerated beam of ^{12}C was delivered to a solid carbon target of 40 $\frac{\mu g}{cm^2}$ and gammas from all decays could be measured. Distinguishing between particle decays and radiative captures could be achieved as particle decays emit a single low

energy gamma and radiative captures emit multiple low energy gammas or a single high energy gamma. By using Monte Carlo simulations to estimate the efficiency of the Gammasphere at detecting low energy gammas, a cross-section for cascade decays of radiative capture could be estimated. However, due to detector saturation, observation of single decays from radiative captures was not possible.

All these problems can be avoided with a facility like DRAGON. With the DSSSD after the EMS, which can be used to select ^{24}Mg and to separate the various particle decay recoils, one can isolate radiative capture events. Also the BGO array will not saturate under the 20 MeV gammas produced by the single decays. Together, this would allow for the branching ratios between cascade decays, through the important 'doorway' states, and single decays to be quantified for the first time ever. Not only would this increase the knowledge of HIRC, but it could also possibly provide insight into exotic nuclear shapes.

For HIRC experiments, DRAGON would have to be modified to run with solid targets, a feat never performed before. A carousel would be constructed, which could be mounted inside the target area of DRAGON and would house solid carbon targets and apertures to be used for tuning the facility. Still, as neither solid target experiments nor experiments with gammas at energies this high have been performed before on DRAGON, other problems may be encountered. For example, with resonance energies in ^{24}Mg at 6.0, 6.7 and 8.0 MeV, and associated excitation energies of 20.0, 20.7 and 22.0 MeV, new problems are posed for DRAGON. As the facility was designed for lower energies, the dimensions of the BGO array was not designed to detect gamma rays of 20 MeV. These high energy gammas may not be fully captured in the array and may more often pass through the scintillators. Also, as the recoil magnesium decays, it will receive a momentum boost from emitted gammas in the plane perpendicular to the beam axis, which is dependant on the energy of the emitted gammas. The momentum boost from these high energy gammas may be too high and thus push the recoil out of the acceptance range of DRAGON.

Just as Monte Carlo simulations of the Gammasphere were performed to answer efficiency questions, Monte Carlo simulations of DRAGON must be performed to examine the efficiency issues surrounding the $^{12}C(^{12}C,\gamma)$ reaction. These simulations will be based on existing simulations of DRAGON performed in GEANT, a physics simulation library. Changes in the facil-

ity will also need to be changed in the existing simulations. These changes involve the geometry of DRAGON, the addition of solid targets and several others that are outlined later. The purpose of this report is to present the efficiencies for both recoil magnesium through the separator and for the emitted gammas captured by the BGO array.

1.3 GEANT

To further the understanding of DRAGON, computer simulations of the facility are often employed. These simulations have been used for a variety of reasons ranging from exploring detector designs to understanding experimental results. They were designed with GEANT version 3.21, a program developed at CERN. GEANT is a package of utilities that was originally designed to assist in simulations of high energy elementary particles moving through matter, but has been expanded for other applications including nuclear physics. The package contains specialized methods and functions to simulate physical processes, which users can incorporate into simulations of experimental setups [5].

GEANT has two main features. The first is constructing experimental setups in simulations. Setups can be defined by piecing together series of basic geometric volumes, such as simple boxes and cones or more complex volumes such as hyperbolic tubes or twisted trapezoids. These volumes are constructed in user geometry files, such as *ugeom_gbox.f* and *ugeom_trgt.f*, using the GEANT method GSVOLU. For each volume a tracking medium is specified from a list of defined media in the user medium file, *ugstmed.f*. A medium definition specifies tracking parameters, such as step sizes, and a specific material type. Material types are defined in user material files, such as *ugmate.f*, which specify the physical properties of a material. Fundamental material properties, such as atomic weights and proportions of constituent elements, are required to be defined. Once a volume has been constructed it is positioned, by calling the GSPOS method in the geometry files, in either the simulation's WORLD or inside a previously constructed and positioned volume.

For simulations of DRAGON, the geometry was split into two areas, a detector area and a separator area. The detector area contained the target box, the BGO array and all the collimators and pumping tubes before the entrance of the first quadrupole. This area was hard coded into the *ugeom_gbox.f* and *ugeom_trgt.f* user geometry files. The separator area contained the remaining components of DRAGON, everything after and including, the first quadrupole. This area was designed using a program called RAYTRACE and is read-in during initialization. The parameters for this part of the geometry are read from the *dragon_2001.dat* file, which must be referenced in the MITRAY environment variable. The construction and po-

sition of volumes is then preformed in *mitray_setup.f*. The separator area of DRAGON was constructed in this manner so that magnetic and electrostatic elements, all of which are contained in the separator area, can be scaled for the recoils of the reaction being studied. The complete GEANT representation of DRAGON is displayed in figure 3. For comparison, figure 3 is in the same orientation as figure 1, with the target area positioned in the top left of the image.

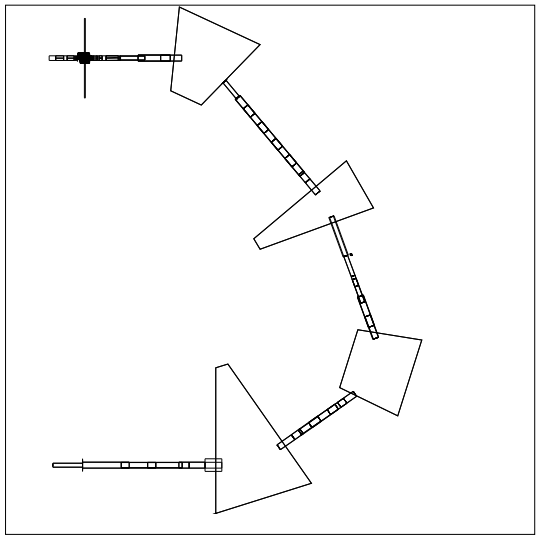

Figure 3: Layout of Simulated DRAGON.

The second main feature is the tracking of particles through the designed geometries. GEANT transports particles through volumes on a step-by-step basis, with the step size defined by a volume's medium, while considering a variety of circumstances. It considers volume boundaries and how various types of particles interact with those boundaries. For example, if a recoil atom that is stepping through the vacuum inside a collimator steps across the boundary of the aluminum collimator, the recoil will lose all its energy and stop. A gamma ray, under the same circumstances, would not stop immediately at the boundary between vacuum and aluminum. It would continue to step through the aluminum and at each step interaction probabilities would be considered. GEANT also takes into account magnetic and electrostatic fields at each step. At the start of each step, ionized recoils will have their

momentum components adjusted based on well understood electromagnetic laws programmed into GEANT. It also simulates the response of materials defined as detectors. For example, with BGO defined as a sensitive detector in *ugmate.f*, gamma rays that enter BGO will Compton scatter, create scintillation electrons and electron-positron pair produce. These processes are also based on well understood laws and incorporate Monte Carlo generators. Every new particle is placed in a queue, with its position and momentum, to be stepped when the original gamma ray stops. Any energy lost in a sensitive detector such as BGO is recorded by GFHITS and can recalled and analyzed similar to experimental data later in the simulation. A reaction's simulated track is presented below in figure 4.

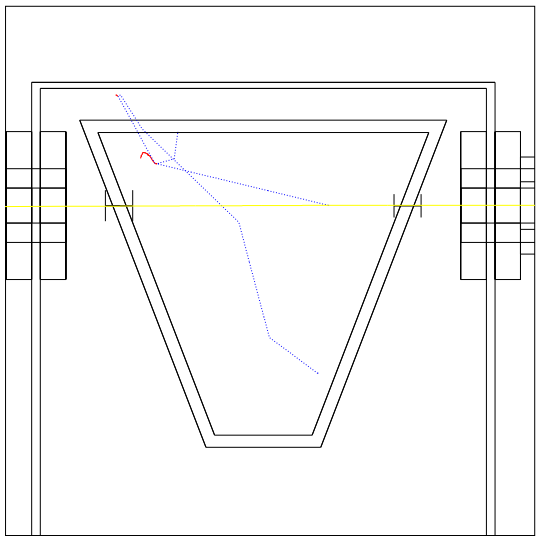

Figure 4: Simulated Particle Tracks Through Gas Cell.

A beam particles enters the gas cell from the right (yellow track). It reacts with the target gas and creates a recoil which decays a moment later and emits a gamma ray. The recoil continues out of the gas cell (yellow track) and the gamma (blue track) heads towards a BGO (not drawn) where it scatters and pair produces creating a shower of photons (blue track), electrons (blue track) and positrons (red track).

While GEANT performs the above mentioned tasks very well, much work is still left up to the user. GEANT requires code to describe the environment of the experimental setup. For example, positioning a volume of target gas inside the windowless gas cell will not cause any leaky gas to escape up and downstream. A volume for each different gas pressure and density must be constructed and positioned separately.

While most of the stepping is performed by GEANT, the program does allow for user stepping files such as *gustep_trgt.f* and *gustep_mitray.f*, which can contain extra conditions. Often there are specific data one wants to record during simulations or specific conditions to consider as a particle steps. These files are where such code is usually stored. For example, when a beam particle steps through the target volume GEANT is not designed to consider the nuclear reaction. Cross sections considerations must be designed by the user. Then should a reaction occur, the beam particle must be manually stopped and the resonant particle must be created with the same position and proper momentum.

Data handling is also left to the user. For DRAGON, simulations analysis is performed during run-time on either a step-by-step basis or in routines called at the end of each event. Results are plotted in one and two dimensional histograms using CERN's HBOOK package version 4.22 [6]. These are stored in HBOOK files that are later viewed using CERN's PAW version 2.13. Declarations of one and two dimensional HBOOK histograms are performed with the methods HBOOK1 and HBOOK2 respectively in *uhinit.f*. Histograms can be incremented using the HFILL method. Analysis on a step-by-step basis can be performed in the user stepping files described above. This is generally used for simple analysis similar to retrieving a recoil's energy when it reaches the DSSSD or for calculating the time of flight between two volumes and incrementing the appropriate histogram. Analysis performed at the end of an event is done in *gudigi.f*. More complex analysis that involves retrieving values from several parts of the simulation is usually performed in this file. This would be similar to counting the total number of BGOs triggered during the event with a recoil reaching the end detectors.

Most important, GEANT is not an executable program in itself. It is a library of methods involving physical processes that greatly assists building real executable simulations

2 GEANT Simulations

In order to simulate the response of DRAGON in GEANT for the $^{12}C(^{12}C,\gamma)$ reaction, several features had to be added to the simulation. The first was the design of ^{24}Mg nuclear structure, which was done in the *c12c12g.dat* input file. It was designed to have a mass of 13.93 MeV less than 24 amu, by changing the recoil_mass_excess variable, and was designed with two energy levels above ground state. The first state was set at 10.0279 MeV above the ground state. The energy of the second state, which was set as the resonance state by setting the rstate variable, was changed between 20.0, 20.7 and 22.0 MeV, one energy per simulation. These states had corresponding resonance energies of 6.0, 6.7 and 8 MeV as seen in the energy diagram in figure 5. All three resonances were examined during experiments and it was observed that all three resonance states decayed to the 10 MeV state, justifying the inclusion of only one resonance state per simulation. The simulations presented in this report all used the 20.7 MeV state.

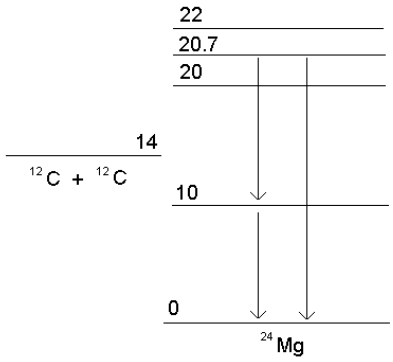

Figure 5: Energy Diagram for $^{12}C(^{12}C,\gamma)$.

A pure carbon material was also designed to be used as a target. The standard properties of carbon were set in the user's materials file, *ugmate.f* and tracking parameters were set in *ugstmed.f*. The target thickness used in some experiments and all simulations was 44 $\frac{\mu g}{cm^2}$. During initial simulations with this target, GEANT stepped through it in one or two steps. To force GEANT to take more steps through the target, the density of carbon was decreased 100 fold in *ugmate.f* to 2.25 $\frac{cg}{cm^3}$ and the length of the target was

similarly increased. The length of the target was calculated as below.

Target length: $\frac{44\frac{\mu g}{cm^2}}{2.25\times10^6\frac{\mu g}{cm^3}} = 19.83 \times 10^{-6}$ cm
Exaggerated 100x: 19.83×10^{-4} cm

The energy of the incoming beam had to be set as well. For the reaction to take place in the center of the target, the energy in the center of mass of the system at the center of the target had to be 6.7 MeV. The calculation of the required beam energy is displayed below. Beam energies for simulations were set to 13.80 MeV by setting the BEAM ffcard in the *dragon_2003.ffcards* input file. This was the energy used during experimental runs.

Required E_{CM} at target center: 6.7 MeV
E of ^{12}C beam at target center: (6.7 MeV)($\frac{24amu}{12amu}$)=13.4 MeV
Adjust for ^{12}C E loss in target: 13.4 MeV+0.33 MeV=13.73 MeV
(From DRAGON log book)
Initial E of beam: 13.73 MeV

More than just the properties of the beam, target and recoils had to be designed. The actual geometry of DRAGON in the simulation had to be changed for solid target experiments. Typically, DRAGON runs with a windowless gas cell inside the target chamber but for the solid target simulations the gas cell was removed and replaced with a solid target disc. The gas cell volume, CELL, and its constituents, CELG, EAPG and XAPG, were removed from *ugeom_trgt.f* and the target disc volume, CTAR, was added to *ugeom_gbox.f*. See figures 6 and 7. In experimental runs, the solid target is held in place by an aluminum carousel. This carousel was designed to not obstruct the path of the recoil magnesium and simulations showed that a similar amount of aluminum did not significantly attenuate emitted gammas. The carousel was therefore not placed in the simulation. Also, when a windowless gas cell is used, there is a small amount of gas leakage up and downstream of the target. Original DRAGON simulations had volumes of decreasing densities of target gas leaking out from the target in *ugeom_trgt.f*. These were changed to vacuum for solid target work.

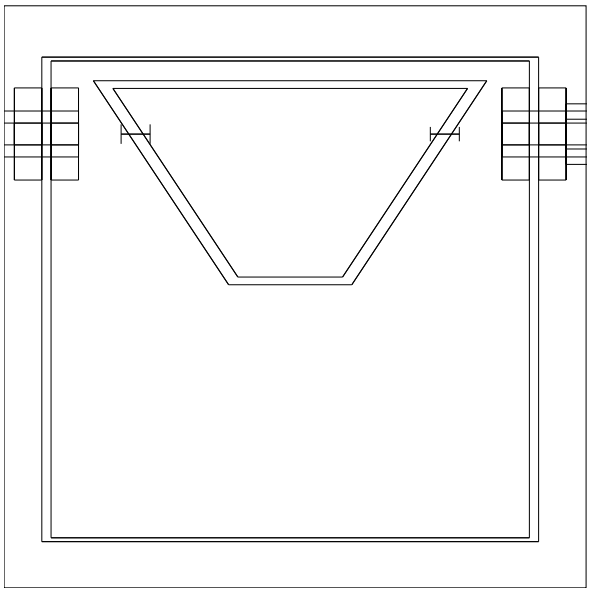

Figure 6: Gas Target Geometry.

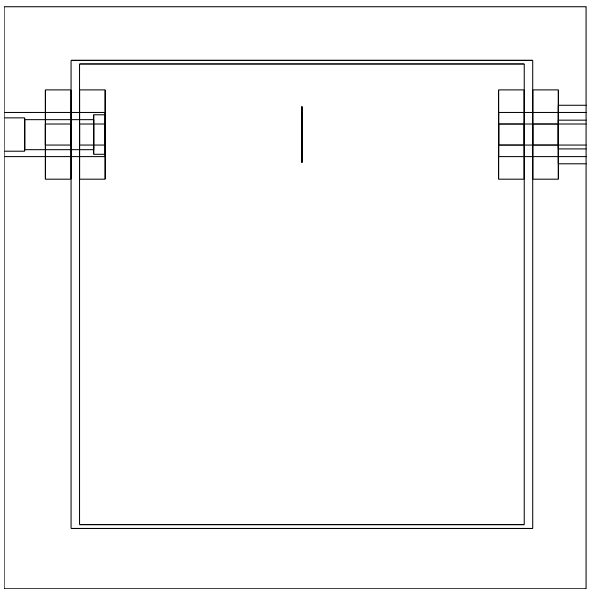

Figure 7: Solid Target Geometry.

The geometry downstream of the target was also changed. Larger collimators and pumping tubes were built for DRAGON to increase the percentage of recoils accepted into the separator. The collimators and pumping tubes were designed in *ugeom_gbox.f* and *ugeom_trgt.f* respectively and, for organizational reasons, a new file called *ugeom_defin.f* was added to contain the dimensions of the collimators and pumping tubes. Although Dr. Trinczek had designed the new geometry for GEANT it was not fully implemented because of problems with the third downstream pumping tube. It was far enough downstream that it protruded into the magnetic field produced by the first quadrupole. Traditionally, the target and gamma detector area, DETE, had been kept separate from the separator area, MITRAY, and this overlap of the two caused problems with GEANT interpretation of magnetic fields in the third pumping tube. The initial solution was to remove the third pumping tube from simulations but before the simulations presented here were run this problem was fixed by building a hollow cone inside the quadrupole inside the separator geometry in *mitray_setup.f*. The old and new collimators and pumping tubes can be seen in figures 8 through 11.

To increase the versatility of the DRAGON simulations two new ffcards were added to *ugffgo.f* and set in the *dragon_2003.ffcards* input file. The value of the first ffcard, named TARG, sets the target geometry as either gas target geometry or solid target geometry during the simulation's initialization. The second, TUBE, selects the collimator and pumping tube dimensions from *ugeom_defin.f* also during initialization. More collimator and pumping tube geometries can be added to this file with ease.

The last main addition to the GEANT simulations was a powerful HBOOK ntuple. An HBOOK ntuple is a table of values, one row per event, which can be plotted during analysis. Basic plotting commands are outlined below and a complete list can be found in the PAW reference manual. This differs from an HBOOK histogram, which is plotted during the run and only during analysis can it be viewed. The new ntuple, #1001: GAMMAHIT, was designed in *gammahit.inc* and declared in *uhinit.f*. It records data relevant to the response of the BGO array. The basic data recorded for each event is the number of BGOs triggered, the total energy deposited in the array and the number and energy of the first and second most energetic BGOs. During simulations these values are calculated after each event in *gudigi.f* and added to the ntuple in *interact.f* using the method HFNT. Two tools were also added to increase the ntuple's power. In user stepping file

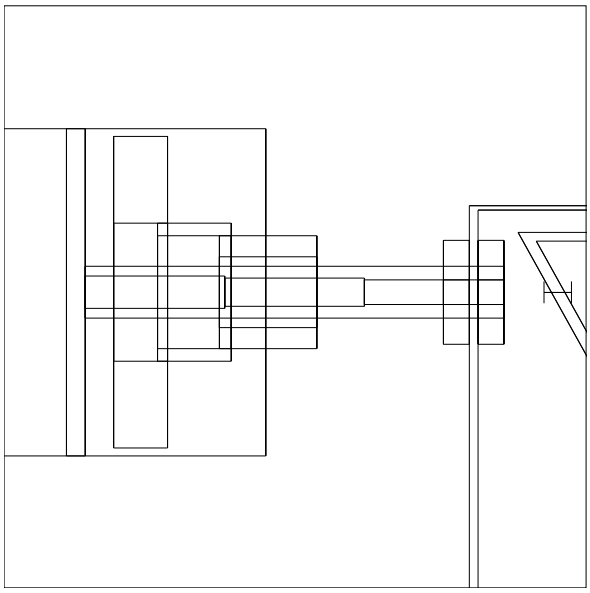

Figure 8: Original Smaller Collimators.

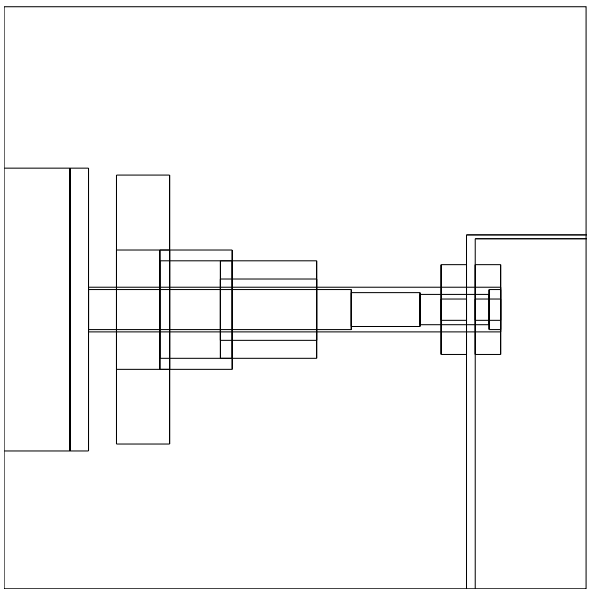

Figure 9: New Larger Collimators.

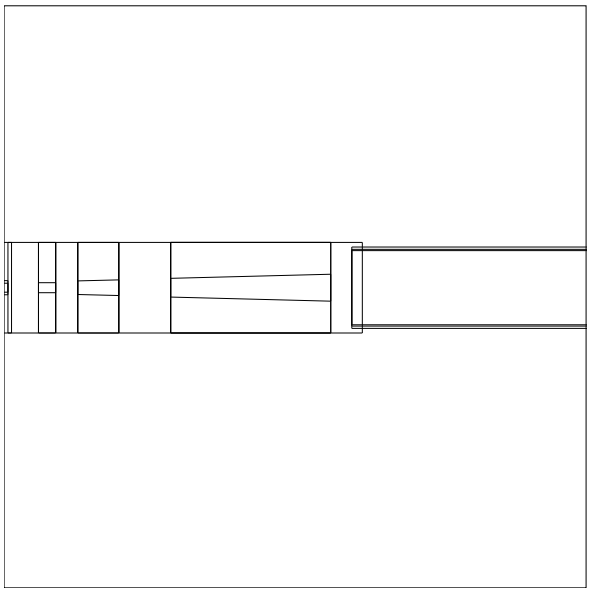

Figure 10: Original Smaller Pumping Tubes.

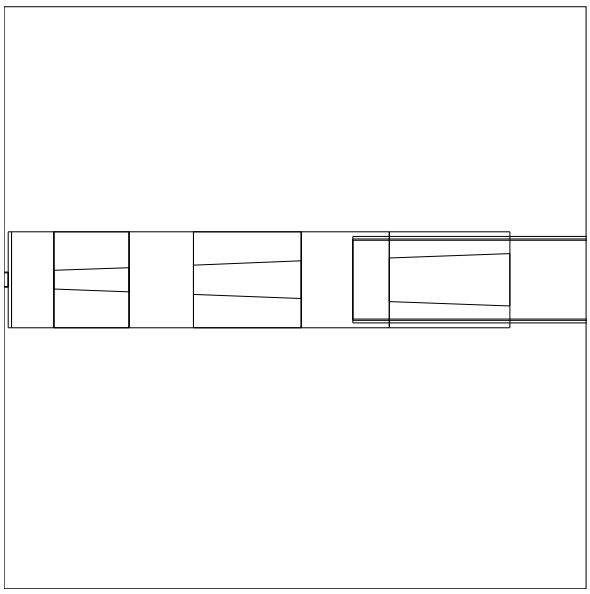

Figure 11: New Larger Pumping Tubes.

gustep_mitray.f the ntuple records whether or not the event's recoil reached the detectors at the end of DRAGON, which allows one to create plots of GAMMAHIT data using only events where a recoil was detected. The second tool is the ability to study any of the above values with 'nearest neighbour adding back'. When high energy gamma rays, particularly the 20 MeV gammas of the $^{12}C(^{12}C,\gamma)$ reaction, interact with BGO, they are likely to produce a shower of electron and positron pairs and Compton and scintillation electrons and photons that can spill over into neighbouring BGOs. With the adding back option, the ntuple will find the BGO with the highest energy and then inspect the energies of all neighbouring BGOs. Any energy deposited in the neighbours is considered to belong to the initial high energy BGO. The energy is subtracted from the neighbours and added back into the high energy BGO. The process repeats by finding the BGO with the next highest energy from the remaining hits. These calculations are performed in *gudigi.f*. Dr. Hutcheon and I defined which pairs of BGOs were to be considered neighbours and developed an adjacency matrix. This matrix is defined in *ugeom_gbox.f* immediately after the BGOs are positioned in the simulation. The overall effect of adding back is a lowering of the reported number of BGOs triggered.

Ntuple plotting commands
Plot 1-D histogram
nt/pl 1001.x

Plot 2-D histogram
nt/pl 1001.y%x
Plot histogram of events meeting specific conditions
nt/pl 1001.y z.gt.1

Create new histogram to define binning parameters
1dhisto 999 'new histo' Xnum Xmin Xmax
2dhisto 999 'new histo' Xnum Xmin Xmax Ynum Ymin Ymax

project ntuple plot onto new histogram
nt/project 999 1001.x
nt/project 999 1001.y%x

Where x, y and z are variables recorded in the Ntuple. These can be viewed by double clicking on the Ntuple in the PAW Main Browser

Several problems with the DRAGON code were found and fixed before the simulations presented here were run. For example, positrons would be produced through pair production when gammas interacted with the BGOs. Occasionally they were not captured in the detector area and reached the field of the first magnetic dipole. This caused several errors in GEANT and a loss of event data. This was fixed with a conditional in *gustep_gbox.f* that manually stops any particle, other than beam or recoils, which leaves the detector area. This was an acceptable solution because currently there is no desire to study the interactions of gammas, electrons or positrons with the separator. Also, when one ran the original DRAGON pawlogon file, a PAW macro named glogon was called and it would set GEANT to produce gammas around the target, not beam particles or recoils. This macro call was removed. Next, due to a mix up of coordinate systems during original development, the numbering of the BGOs in the simulation was a mirror image of reality. Their numbering was reversed by positioning the detectors into the simulation in the opposite order in *ugeom_gbox.f*. And finally, the material type of the gamma detectors was not bismuth germanate, but barium fluoride. This was due to an ffcard, DMAT, which overrode the detector material type set in *uvinit.f*. This ffcard was changed to the proper material.

3 Discussion

To examine the differences between cascade decay and single decay recoils in the $^{12}C(^{12}C,\gamma)$ experiment, simulations studying the acceptance of DRAGON for various energy tunes were run. The acceptance is the percent of recoils that are recorded in the DSSSD at the end of DRAGON with respect to the number of reactions and, as described earlier, the facility can be tuned to allow particles of specific energies through the separator. For simulations, this tune can be changed by adjusting the 5^{th} parameter of the ffcard MTUN in *dragon_2003.ffcard*. It was varied from -15% to 15% of expected recoil energy in 1% steps. The percent of recoils detected for each tune was compiled into the plots of acceptance of DRAGON versus energy tune in figures 12 and 13 below. In both figures diamond points represent recoil singles and squares represent recoil-gamma coincident events.

The acceptance for the cascade decay, in figure 12, follows a Gaussian distribution reasonably well and peaks close to the expected energy of the recoils. This is as expected because the recoils emitted two gammas of very similar energies. The magnitude of the momentum of these gammas along the beam axis translates into forward momentum gains and losses for the recoil. For example, if a gamma is emitted in the forward direction, the recoil will lose forward momentum. With two gammas being emitted these gains and loses will, on average, cancel out. This produces the quasi-Gaussian distribution with an average recoil that has not been significantly perturbed from the expected recoil energy, as seen in figure 12. These recoils should easily transmit through DRAGON and hence the highest acceptance is a tune near the expected energy. Interestingly, this peak is at the -3% energy tune. In Other experiments the acceptance peak has been observed at the -1% energy tune. This difference has not been explained.

The acceptance for single decay recoils is significantly different from the acceptance for cascade decay recoils. The first such difference is the location of the acceptance peaks. Figure 13 displays a non-symmetric bimodal distribution for the acceptance of DRAGON. The bimodal distribution is expected because of the single emitted gamma. As the gammas follow a quadrupole distribution they are not likely to be emitted perpendicular to the beam axis. Also with only one emitted gamma no averaging out can take place as seen in the cascade decays. While the bimodal nature of the plot is understandable, the non-symmetric nature has yet to be explained.

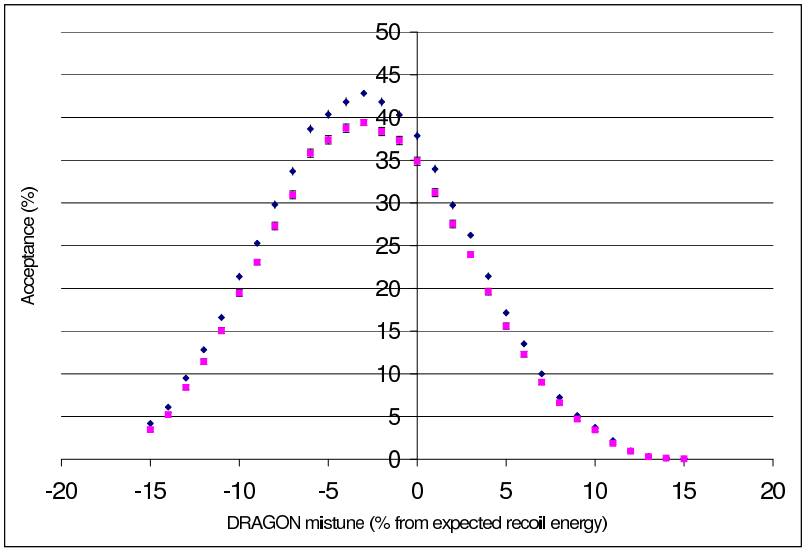

Figure 12: DRAGON acceptence as a function of energy tune for cascade decays.

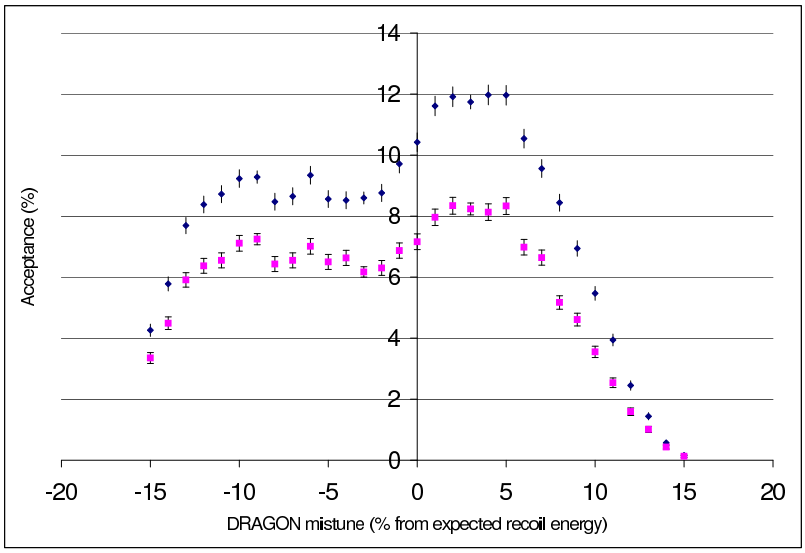

Figure 13: DRAGON acceptence as a function of energy tune for ground decays.

To verify the above interpretations three simulations were more closely examined for both cascade and single decay recoils. These were the simulations with energy tunes at the three peaks in figures 12 and 13, which were +3%, -3% and -9% of expected recoil energy. Plots of the angle theta, which was defined as the angle between the emitted gamma ray and the beam axis, were created in figures 14, 15 and 16. Dashed lines inside the solid curve show the values of theta for detected recoils only. Figures 14 and 16 demonstrate that the recoils being detected at the +3% and -9% energy tunes were recoils that emitted gamma rays predominantly in the backwards direction (a gain in momentum) and forwards direction (a loss of momentum), respectively. Figure 15 illustrates that the angle of the emitted gamma rays at the -3% tune are symmetric around 90°. This is in agreement with the above interpretation.

Out of curiosity, the number of the BGO that registered the highest energy for each event was also plotted in figures 17, 18 and 19. Again, dotted lines inside the solid curve represent BGO number for detected recoils only. It can be seen that recoils being detected at the +3% and -9% energy tunes were recoils that emitted gammas that registered in predominately upstream and downstream BGOs respectively, whereas at the -3% energy tune the triggered BGOs are roughly symmetric. This is also in agreement with the above interpretation. However, there is another asymmetry. For each tune, the detected recoils were more likely to have triggered an even numbered BGO, which are all on the outside of the curve of DRAGON. This asymmetry has also not been explained.

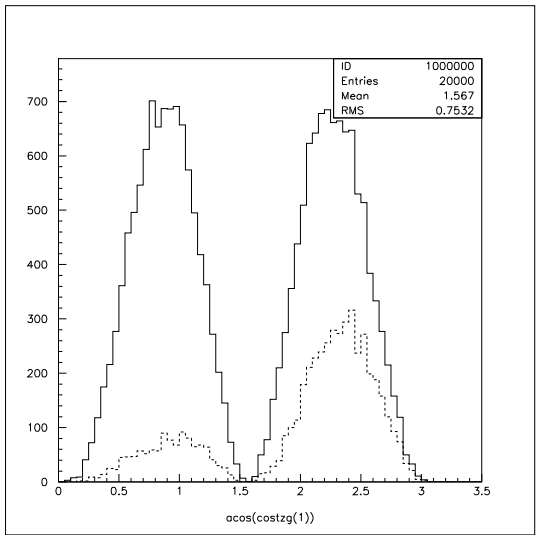

Figure 14: Angle of emitted gamma measured from downstream beam axis with dotted line for coincident events of +3% energy tune.

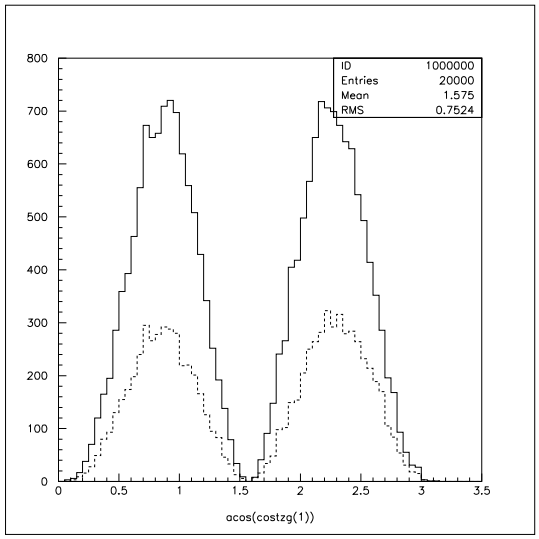

Figure 15: Angle of emitted gamma measured from downstream beam axis with dotted line for coincident events of -3% energy tune.

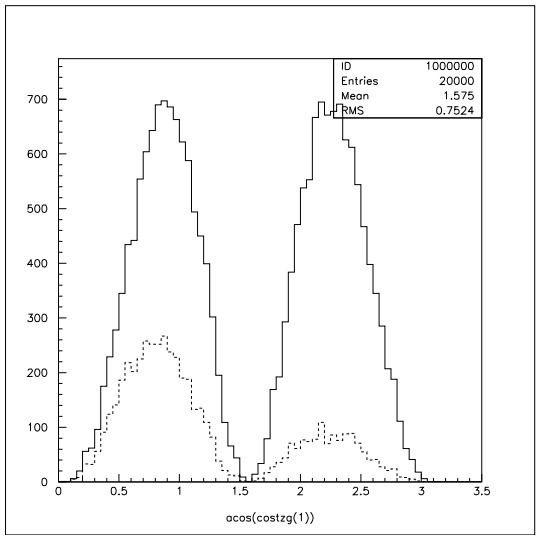

Figure 16: Angle of emitted gamma measured from downstream beam axis with dotted line for coincident events of -9% energy tune.

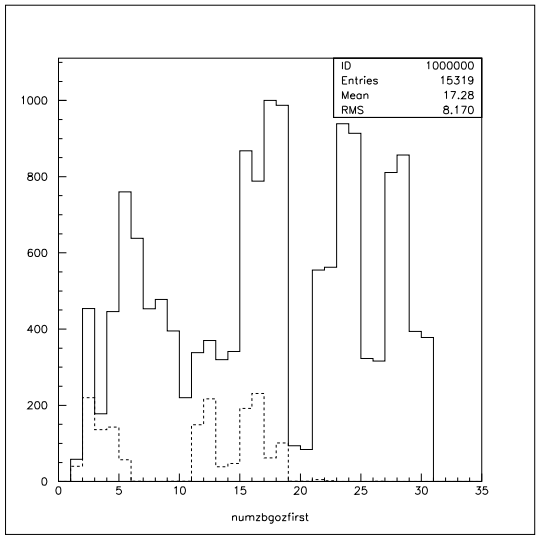

Figure 17: Most energetic BGO number with coincident events with dotted line for coincident events of +3% energy tune.

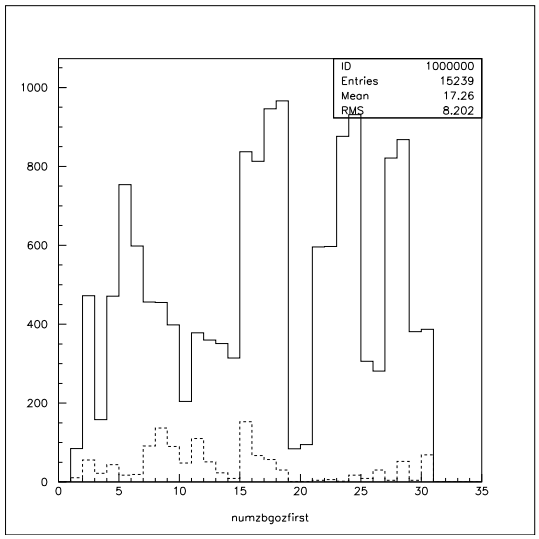

Figure 18: Most energetic BGO number with coincident events with dotted line for coincident events of -3% energy tune.

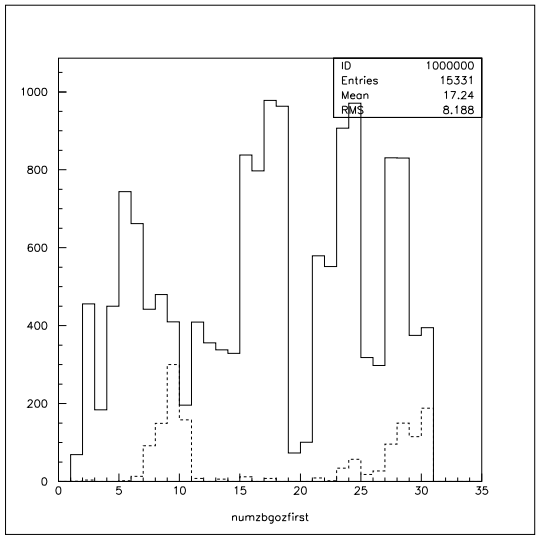

Figure 19: Most energetic BGO number with coincident events with dotted line for coincident events of -9% energy tune.

Another significant difference between the acceptance plots of the two decay patterns is the heights of the various peaks. The cascade decay has a maximum acceptance of nearly 45% whereas the single decay peaks at around 12%. Just as the location of the peaks is related to the magnitude of the emitted gamma rays along the beam axis, the heights of the acceptance peaks are related to the magnitude of the emitted gamma rays in the plane perpendicular to the beam axis. When a recoil emits a gamma with a large perpendicular momentum component, the recoil gains momentum perpendicular to the beam axis. This causes the recoil to travel at an angle away from the beam axis, instead of parallel. If the momentum, and hence the angle, is too large then the recoil will not pass through the openings of the collimators and pumping tubes and will not reach the separator. With cascade decays these components can average out and result in an average recoil that has not been perturbed from the beam axis. Recoils with single decays cannot average out and hence are almost always angled away from the beam axis. Figures 20 and 21 display positions of recoils in the plane perpendicular to the beam axis. It can be seen that the majority of recoils with cascade decays are on the beam axis whereas there is an obvious minimum of single decay recoils on the beam axis. Also to help explain the larger loss of recoils for single decays, a series of pie charts were created in figures 22 through 27. These display the percent of recoils which stopped up in the interval betwen the listed component and the previous component. It is clear from these charts that the majority of single decay recoils are stopped in the downstream pumping tubes as a result of the large perpendicular momentum component. The low acceptance of DRAGON would be a problem in any experimental run of $^{12}C(^{12}C,\gamma)$.

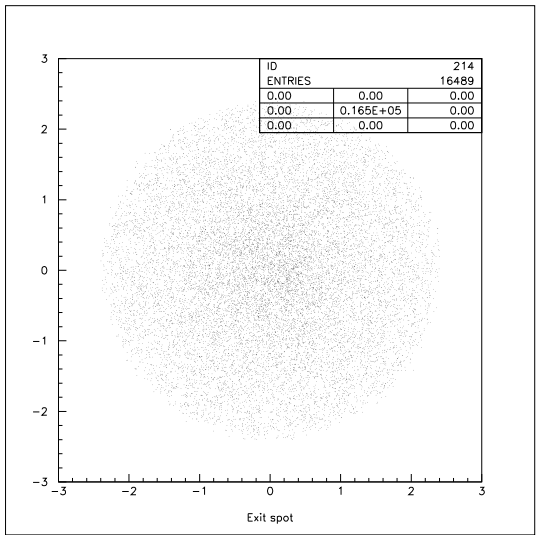

Figure 20: Position of cascade decay recoils in plane perpendicular to beam axis when entering 2^{nd} downstream pumping tube.

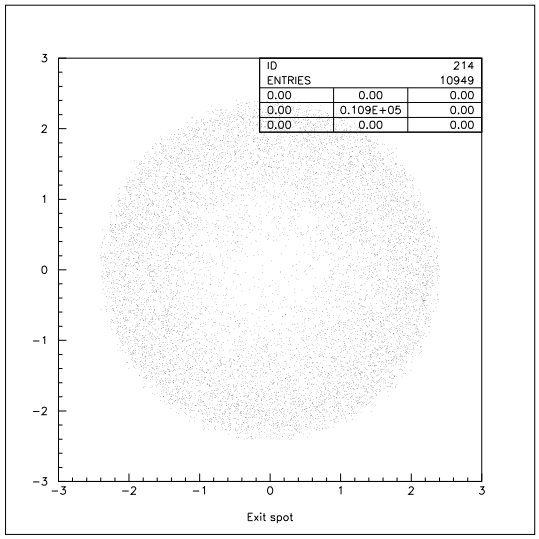

Figure 21: Position of single decay recoils in plane perpendicular to beam axis when entering 2^{nd} downstream pumping tube.

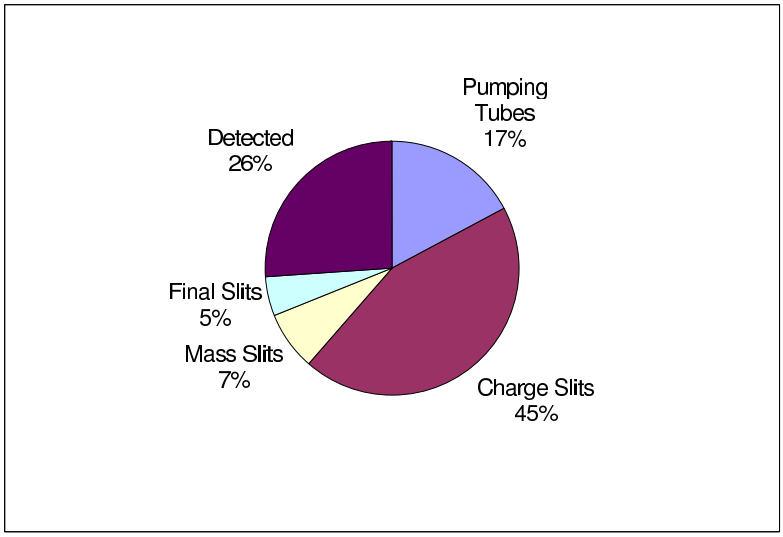

Figure 22: Stopping position of cascade decay recoils with -3% energy tune.

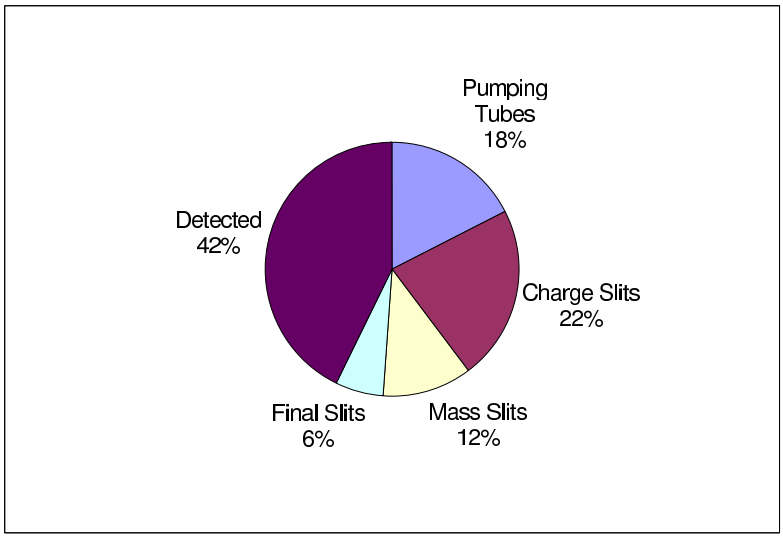

Figure 23: Stopping position of cascade decay recoils with -3% energy tune.

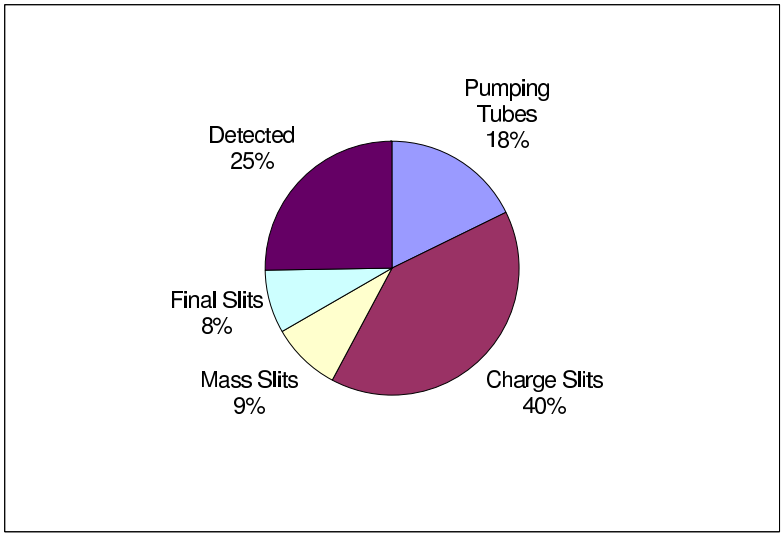

Figure 24: Percent of cascade decay recoils stopped up to with -9% energy tune.

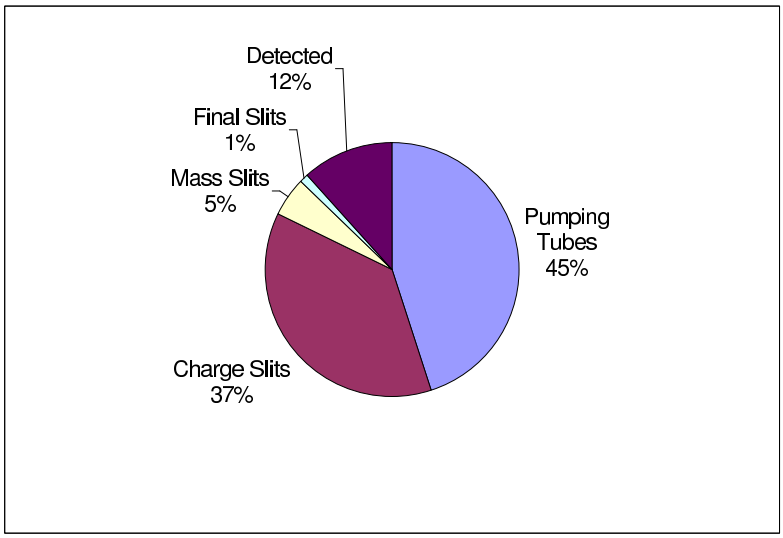

Figure 25: Stopping position of single decay recoils with +3% energy tune.

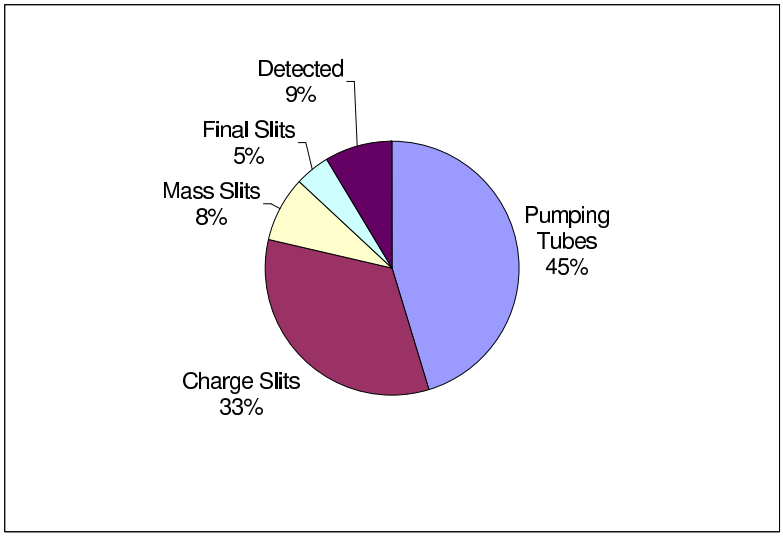

Figure 26: Percent of single decay recoils stopped up to with -3% energy tune.

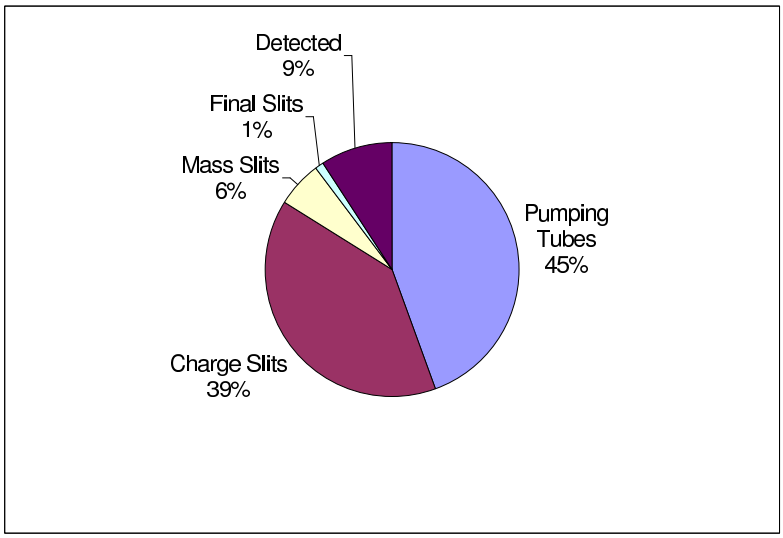

Figure 27: Stopping position of cascade decay recoils with -9% energy tune.

A second set of simulations were run with more events to inspect the response of the BGO array. A simulation was run for all three acceptance peaks, +3%, -3% and -9%, for both cascade decays and single decays. For each energy tune, two plots of energy deposited in the array versus the number of BGOs triggered for events with a detected recoil were made; one with nearest neighbour adding back and one without. These plots are presented in the following pages.

It is clear from these plots that the gamma energy spectra for single decay recoils have a peak at 20.7 MeV, the full energy of the emitted gamma. The number of BGOs triggered, also referred to as the BGO multiplicity, can be as high as 5 or 6 detectors for gamma single events, but only 3 or 4 detectors for coincident events. Employing nearest neighbour adding back reduces this even further and rarely does a coincident event trigger more than 2 detectors.

For cascade decay recoils the gamma energy spectra have 2 clear peaks; one around 10 to 10.7 MeV and one at 20.7 MeV. As the lower peak is much higher a significant number of events have an entire gamma escape undetected. There are also a small number of events with more than 11 MeV detected in a single detector, implying that rarely are both gammas emitted in the same direction. For coincident events there is rarely more than 11 MeV in a single detector. However, with nearest neighbour adding back several coincident events are above 11 MeV in a single detector which, in experimental runs, could be confused with single decay recoils. The multiplicity can also be as high as 5 or 6 detectors for gamma single events, but only 4 or 5 detectors for coincident events, slightly higher than single decay recoils. With nearest neighbour adding back this is reduced to 2 or 3 detectors, still slightly higher than single decays. The difference between cascade decays and single decays in these plots might not be sharp enough to distinguish between the two.

During experimental runs, more information than energy deposited and BGO multiplicity is available for analysis. The following plots are the energy spectra of the most and second most energetic BGO, referred to as γ_0 and γ_1 respectively. It was seen in simulations that these spectra did not change significantly between energy tunes and hence only plots the center tune, -3%, are presented.

The most striking differences between cascade decay and single decay recoils is in the γ_0 and γ_1 spectra. The γ_0 spectrum of coincident events of the cascade decay has very few counts above 11 MeV, only 0.3%. The same

spectrum for the single decay has a much higher 70% of coincident events above the 11 MeV mark. The γ_1 spectra for coincident events also differ significantly. While both have sharp peaks at 0 MeV, meaning a second detector was not triggered, and 511 MeV, a result of pair production, the γ_1 spectrum for cascade decay recoils has a small peak around 10 MeV, whereas the same spectrum for single decay recoils does not. The cascade decay plot also has 57% of counts above 1 MeV whereas the single decay plot has only 25% above 1 MeV. These differences could be used in analysis of experimental data to distinguish between the two decays.

The same plots, but of all events, gamma singles and coincident, show similar differences, but not to the same degree. For example, the γ_0 plots for cascade decays and single decays have 3% and 37% of counts over 11 MeV respectively. As the differences in these plots are not as sharp as in the previous plots, considering only coincident events is probably more useful for any analysis of experimental data.

Employing nearest neighbour adding back adds more useful information to the analysis. The γ_0 spectra have 75% of counts above 11 MeV for coincident single decays and only 4% for cascade decays. The γ_1 spectra are also improved. For cascade decays the 10 MeV peak is sharper and for single decays almost every count is less than 511 keV. The latter implies that the majority of second BGOs triggered for single decays, with nearest neighbour adding back, are the result of pair production. A more detailed look into which BGOs were triggered with 511 keV indicated that these BGOs were generally on the opposite side of the array as the most energetic BGO. This implies that the gamma pair produces when it interacts with the first BGO and one of the pairs travel back through the target to intercept a detector on the other side. Pairs that did not travel back through the target were caught by neighbouring BGOs and were added back.

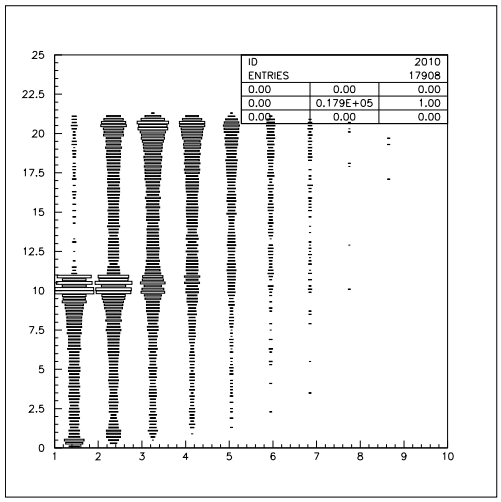

Figure 28: Energy detected in BGO array versus number of BGOs triggered, for all cascade decay events.

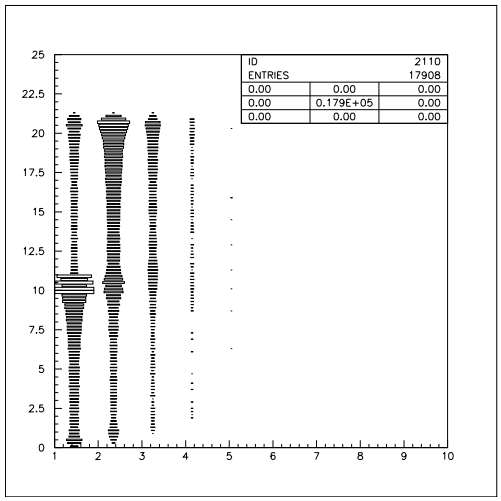

Figure 29: Energy detected in BGO array versus number of BGOs triggered, for all cascade decay events, with nearest neighbour adding back.

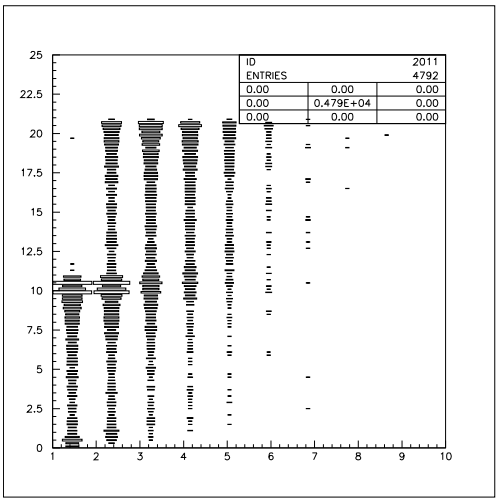

Figure 30: Energy detected in BGO array versus number of BGOs triggered, for coincident cascade decay events with +3% energy tune.

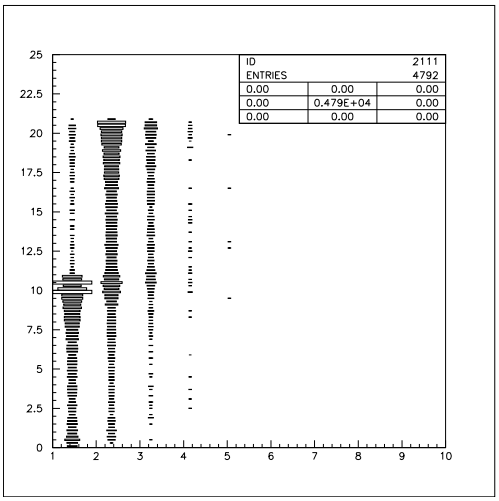

Figure 31: Energy detected in BGO array versus number of BGOs triggered, for coincident cascade decay events with +3% energy tune, with nearest neighbour adding back.

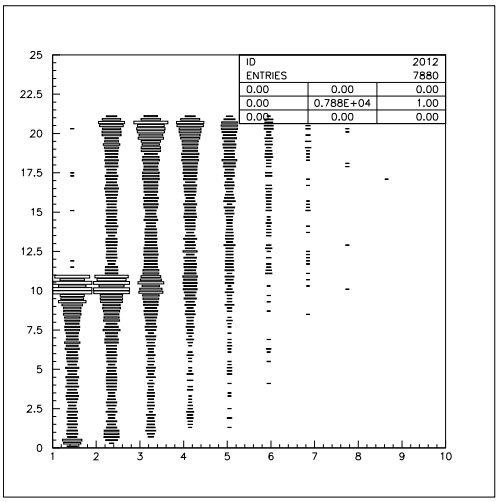

Figure 32: Energy detected in BGO array versus number of BGOs triggered, for coincident cascade decay events with -3% energy tune.

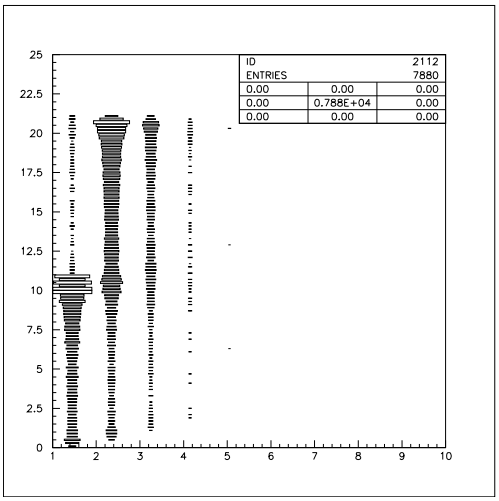

Figure 33: Energy detected in BGO array versus number of BGOs triggered, for coincident cascade decay events with -3% energy tune, with nearest neighbour adding back.

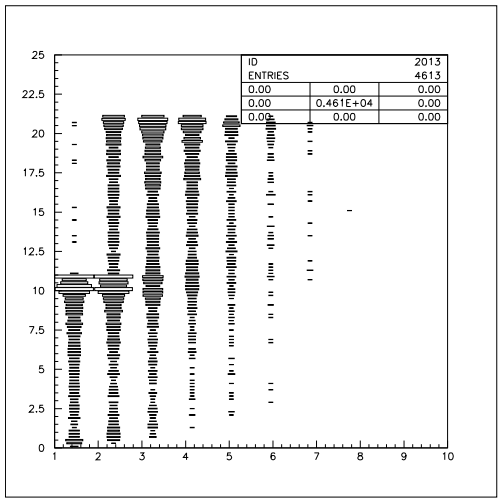

Figure 34: Energy detected in BGO array versus number of BGOs triggered, for coincident cascade decay events with -9% energy tune.

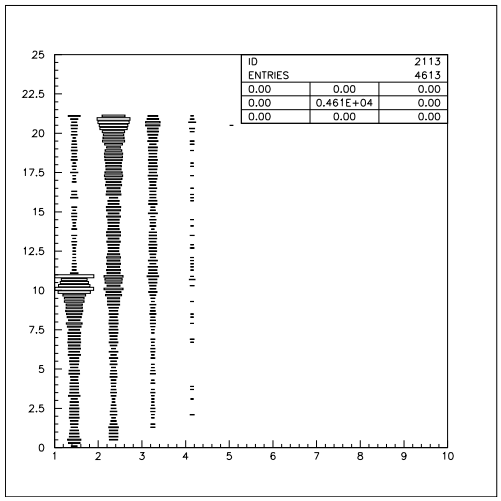

Figure 35: Energy detected in BGO array versus number of BGOs triggered, for coincident cascade decay events with -9% energy tune, with nearest neighbour adding back.

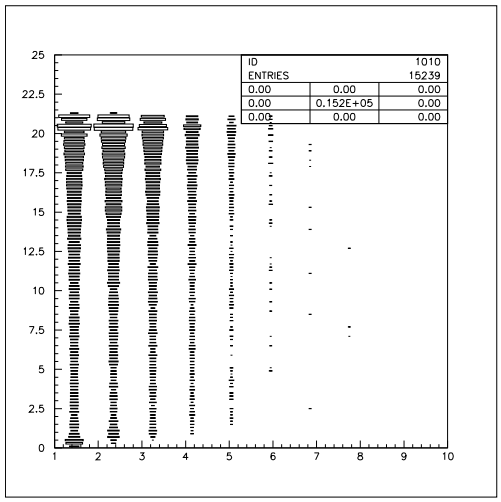

Figure 36: Energy detected in BGO array versus number of BGOs triggered, for all single decay events.

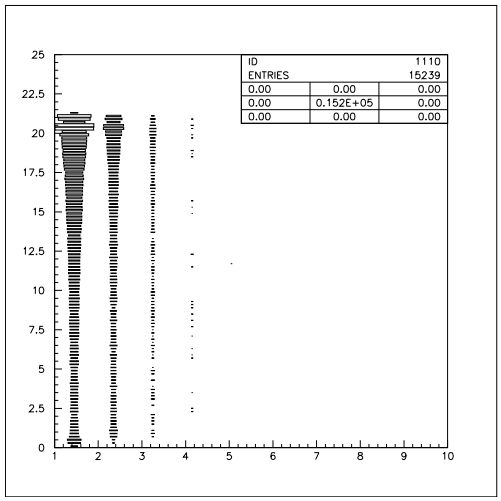

Figure 37: Energy detected in BGO array versus number of BGOs triggered, for all single decay events, with nearest neighbour adding back.

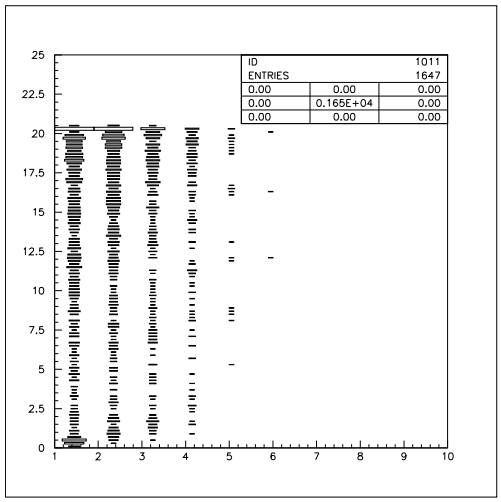

Figure 38: Energy detected in BGO array versus number of BGOs triggered, for coincident single decay events with +3% energy tune.

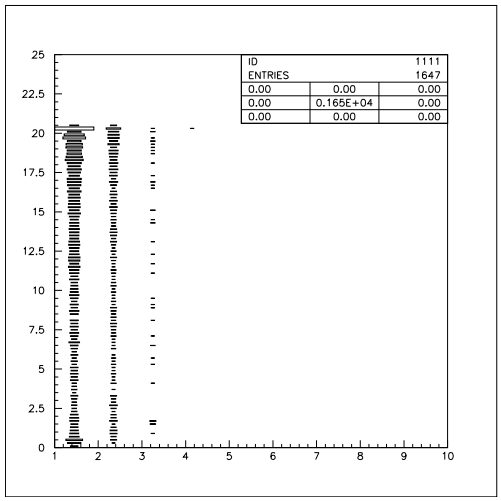

Figure 39: Energy detected in BGO array versus number of BGOs triggered, for coincident single decay events with +3% energy tune, with nearest neighbour adding back.

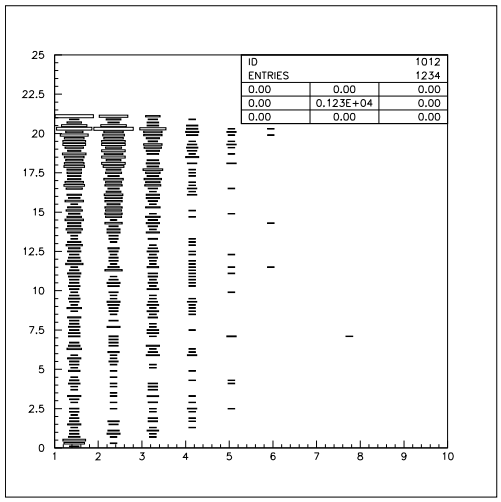

Figure 40: Energy detected in BGO array versus number of BGOs triggered, for coincident single decay events with -3% energy tune.

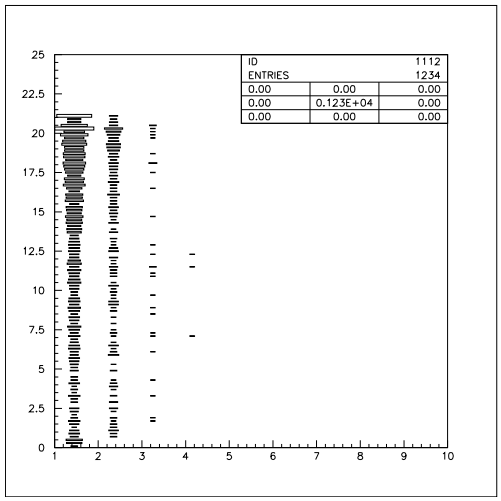

Figure 41: Energy detected in BGO array versus number of BGOs triggered, for coincident single decay events with -3% energy tune, with nearest neighbour adding back.

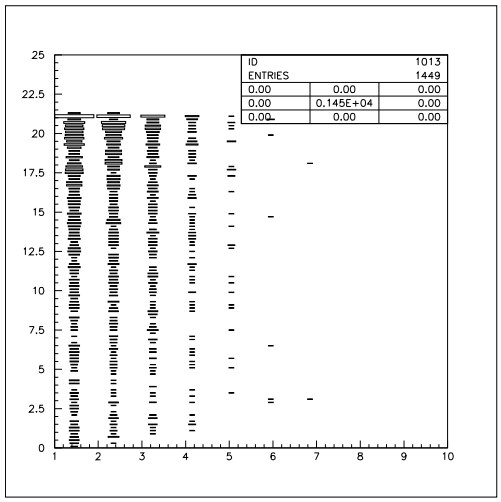

Figure 42: Energy detected in BGO array versus number of BGOs triggered, for coincident single decay events with -9% energy tune.

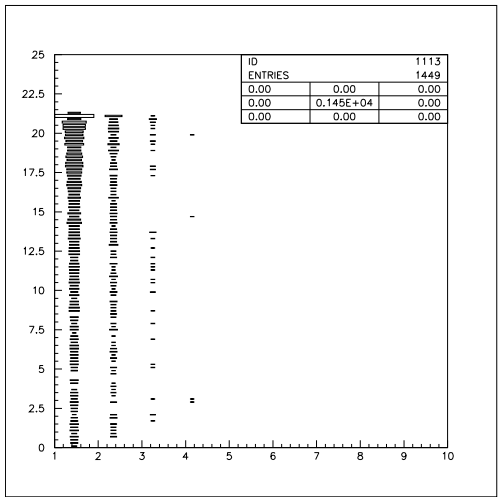

Figure 43: Energy detected in BGO array versus number of BGOs triggered, for coincident single decay events with -9% energy tune, with nearest neighbour adding back.

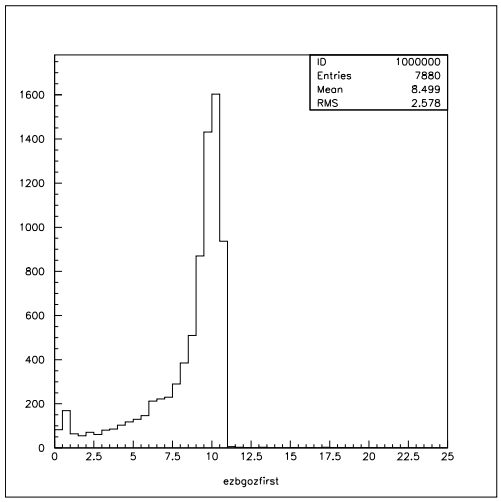

Figure 44: Energy in most energetic BGO (γ_0) for cascade decay events.

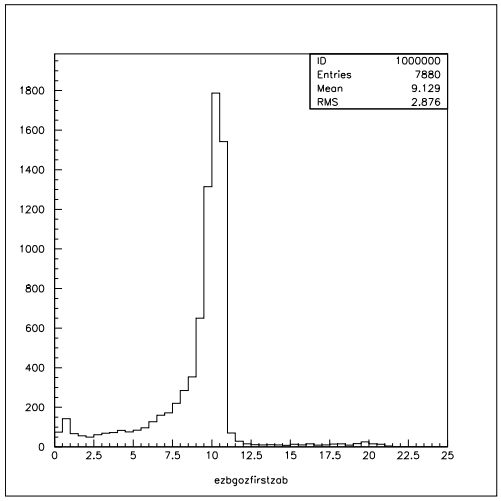

Figure 45: Energy in most energetic BGO (γ_0) for cascade decay events, with nearest neighbour adding back.

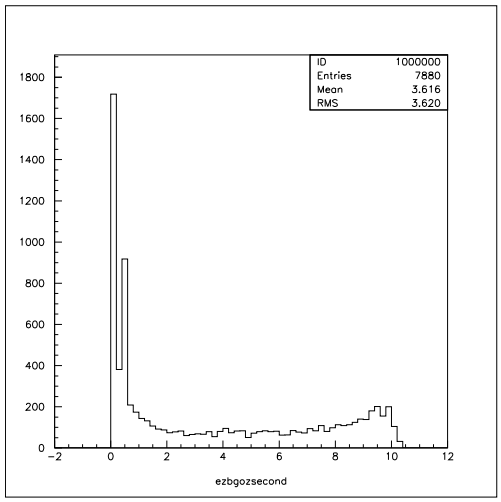

Figure 46: Energy in second most energetic BGO (γ_1) for cascade decay events.

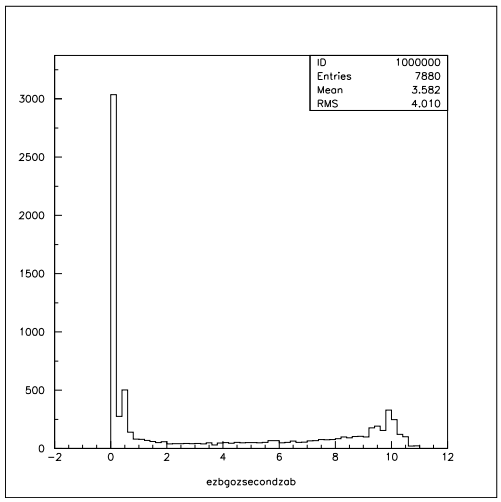

Figure 47: Energy in second most energetic BGO (γ_1) for cascade decay events, with nearest neighbour adding back.

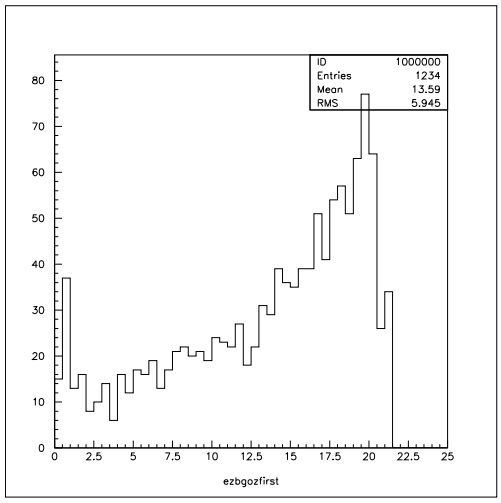

Figure 48: Energy in most energetic BGO (γ_0) for single decay events.

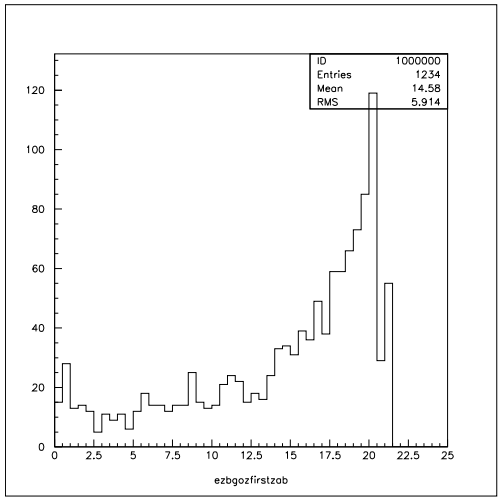

Figure 49: Energy in most energetic BGO (γ_0) for single decay events, with nearest neighbour adding back.

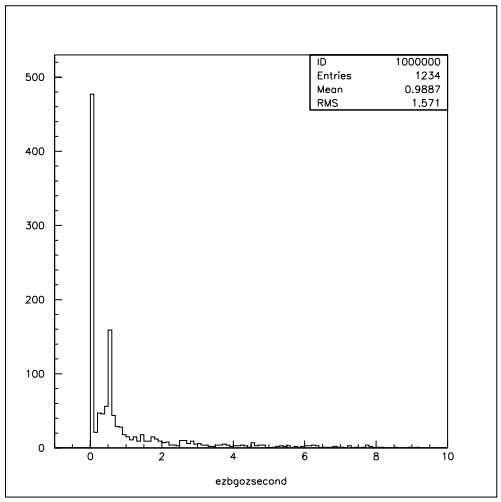

Figure 50: Energy in second most energetic BGO (γ_1) for single decay events.

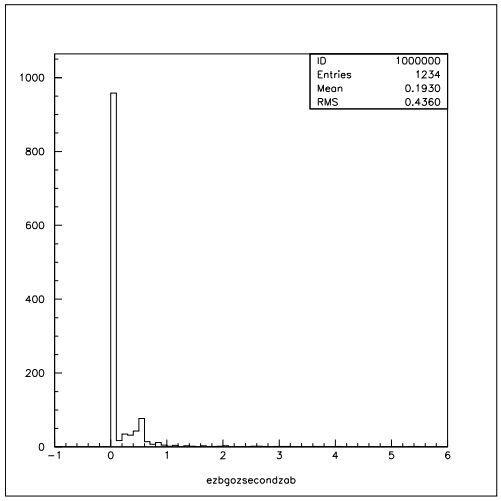

Figure 51: Energy in second most energetic BGO (γ_1) for single decay events, with nearest neighbour adding back.

4 Conclusions and Recommendations

The sharp differences between the γ_0 and γ_1 plots indicate the best way to distinguish between cascade decay and single decay recoils in experimental runs. While it was seen that the nearest neighbour adding back technique sharpened the differences between these plots, a more involved algorithm could be designed and run on experimental data. This algorithm would consider the energy distribution and positions of γ_0 and γ_1 to estimate the number of emitted gammas for each event. This is the key to identifying whether a recoil decayed through a cascade or a single step. These simulations show that for single decays the 20 MeV gamma will deposit the majority of its energy into a single BGO. Although some energy will often be detected in neighbour BGOs and even BGOs on the opposite side of the array, these energies are never as high as γ_0. For cascade decays the two 10 MeV gammas are usually distinguishable. If they trigger BGOs that are spaced apart, γ_0 and γ_1 with nearest neighbour adding back will reflect this. Even if the two gammas trigger neighbouring detectors, the non-added back γ_0 and γ_1 values will be similar. This rarely happens for the 20 MeV gammas of the single decay. The main problem with this method is that the BGO array does not always capture all of the energy from the emitted gammas. If very low energies are recorded in BGOs that are not neighbours, it is likely a cascade decay but low energies in a single detector will not be distinguishable between cascade and single decays. Still, it is recommended that such an algorithm be developed to reconstruct the number of emitted gamma rays for each reaction studied with DRAGON.

It is also recommended that only coincident events be used in analysis. The simulations showed that the number of gammas is more easily reconstructed from coincident events than single events. Efficiencies calculated for recoils and gammas from these simulations and future ones could be used to calculate the properties of the $^{12}C(^{12}C,\gamma)$ reaction. However, as the findings in this report are based on GEANT simulations of DRAGON and analysis of experimental results may be based on these simulation, work should be done to verify the simulations. This could be done by comparing gamma spectra or relative recoil efficiencies between various energy tunes. Testing the accuracy of the simulation in all areas of the facility, BGO array and separator, is very important. A more detailed examination of some of the asymmetries described above could also further the understanding of DRAGON.

References

[1] D.A. Hutcheon *et. al.*, Nuclear Instruments and Methods in Physics Research A 498 (2003) 190-210.

[2] A.M. Nathan, A.M. Sandorfi, and T.J. Bowles, Physical Review C 24, 932 (1981).

[3] A.M. Sandorfi and A.M. Nathan, Physical Review Letters 40, 1252 (1978).

[4] D.G. Jenkins *et. al.*, Experiment 947 TRIUMF Research Proposal (2002).

[5] CERN Application Software Group, GEANT Manual: Detector Description and Simulation Tool (1994).

[6] CERN Application Software Group, HBOOK Reference Manual (1995)